Electroluminescence from Electrolyte-Gated Carbon Nanotube Field-Effect Transistors

Jana Zaumseil,[†,*] Xinning Ho,[‡] Jeffrey R. Guest,[†] Gary P. Wiederrecht,[†] and John A. Rogers[‡]

[†]Center for Nanoscale Materials, Argonne National Laboratory, Argonne, Illinois 60439, and [‡]Department of Materials Science and Engineering, University of Illinois at Urbana–Champaign, Urbana, Illinois 61801

ABSTRACT We demonstrate near-infrared electroluminescence from ambipolar, electrolyte-gated arrays of highly aligned single-walled carbon nanotubes (SWNT). Using electrolytes instead of traditional oxide dielectrics in carbon nanotube field-effect transistors (FET) facilitates injection and accumulation of high densities of holes and electrons at very low gate voltages with minimal current hysteresis. We observe numerous emission spots, each corresponding to individual nanotubes in the array. The positions of these spots indicate the meeting point of the electron and hole accumulation zones determined by the applied gate and source–drain voltages. The movement of emission spots with gate voltage yields information about relative band gaps, contact resistance, defects, and interaction between carbon nanotubes within the array. Introducing thin layers of HfO_2 and TiO_2 provides a means to modify exciton screening without fundamentally changing the current–voltage characteristics or electroluminescence yield of these devices.

KEYWORDS: carbon nanotube · electroluminescence · field-effect transistor · electrolyte gating · ambipolar

In recent years, field-effect transistors (FET) based on single-walled carbon nanotubes (SWNT) have been shown to exhibit a range of interesting optoelectronic effects.[1] In particular, near-infrared electroluminescence (EL) was demonstrated for ambipolar and unipolar field-effect transistors that used either random networks of SWNTs or individual SWNTs.[2–6] In these devices, excitons resulted from the recombination of holes and electrons that were injected from the source and drain electrodes, respectively. However, external quantum efficiencies were generally low (10^{-7} to 10^{-6} photons per electron),[4,5] and many nanotube FETs suffered from current hysteresis due to the presence of water under ambient conditions and the high voltages required for sufficient injection of holes and electrons.[3,7,8] Because nanotubes with large diameters (>1.5 nm) and small band gaps have the lowest injection barriers for both carrier types,[9] they are best suited for ambipolar FETs, and thus electroluminescence is usually observed at wavelengths around 1.8 to 2 μm.[4–6]

In order to make light-emitting carbon nanotube FETs interesting for applications, their device properties have to be improved significantly. Major objectives are minimization of applied voltages and current hysteresis, device uniformity and reproducibility, for example, by statistical averaging over many nanotubes, and optimization of electroluminescence efficiency in the optical telecommunications window by shifting emission toward shorter wavelengths and avoiding quenching caused by metallic nanotubes and substrate effects.

Here we present near-infrared light emission from electrolyte-gated ambipolar field-effect transistors with large scale, parallel arrays of carbon nanotubes grown by chemical vapor deposition (CVD) on quartz substrates. Two aspects of these devices are significant, compared to previous light-emitting nanotube transistors. First, we use high quality, nearly perfectly linear, aligned arrays of SWNTs that have been shown to yield transistors with excellent performance characteristics, high levels of reproducibility in wafer-scale arrays, and demonstrated applications in radio frequency electronics and other integrated systems.[10,11] These arrays provide a multitude of light sources with potential for high overall output. They also offer reproducible properties due to statistical averaging effects owing to the large numbers of tubes in the channel without the drawback of uncontrolled energy transfer and quenching by metallic tubes associated with dense random arrays of SWNT. They are significant for basic scientific study because emission from large numbers of tubes can be evaluated in a single device under identical conditions, thereby allowing systematic investigations of emission properties depending on tube

*Address correspondence to jzaumseil@anl.gov.

Received for review June 1, 2009 and accepted July 20, 2009.

Published online July 27, 2009.
10.1021/nn9005736 CCC: $40.75

diameter, chirality, and other characteristics. Disadvantages of these thin film-like arrays are the presence of metallic nanotubes that cause large off currents and reduce overall efficiency and the inability to determine individual current−voltage characteristics and threshold voltages of the carbon nanotubes in the array.

The other important feature of the light-emitting FETs introduced here is that they use electrolyte gating as a way to achieve high charge carrier densities with drastically reduced gate and source−drain voltages while avoiding current hysteresis, as demonstrated previously in carbon nanotube and organic field-effect transistors.[12−15] In these devices, the gate dielectric is replaced by an electrolyte, for example, imidazolium-based ionic liquid gels or $LiClO_4$ dissolved in poly(ethylene glycol) (PEG). When a negative voltage is applied, positive cations are attracted to and negative anions are repelled from the gate electrode. The cations form an electric double layer at the gate/electrolyte interface, while the anions do the same at the carbon nanotube/electrolyte interface, where they induce accumulation of holes in the nanotube. The bulk electrolyte remains charge-neutral so that almost all of the applied potential is dropped across these electric double layers, which leads to an extremely high effective gate capacitance of tens of $\mu F \cdot cm^{-2}$ and thus high charge carrier densities. Changing the gate voltage causes the ion distribution to re-adjust with diffusion-limited rates. This redistribution avoids charge trapping and associated hysteresis that occur in oxide dielectrics. The strong gate coupling provided by the electrolyte enables efficient charge injection, due to sharp bending of the valence and conduction band at the metal/nanotube interface and thus enhanced tunneling through the thin Schottky barrier. In this manner, both holes and electrons can be efficiently injected even into carbon nanotubes with relatively small diameters (*i.e.*, large band gaps) and under ambient conditions. Simultaneous injection of both charge carriers leads to coexisting hole, and electron accumulation zones along the nanotube and light emission take place at the point where the opposite charge carriers meet and recombine. The position of the recombination zone is determined by the gate and source−drain voltages and thus the local potential along the nanotubes.[3,16,17] We note that electroluminescence from electrolyte-gated SWNTs is particularly interesting because metal ions can quench nanotube luminescence.[18] Here positive (*e.g.*, Li^+) and negative (*e.g.*, ClO_4^-) ions are accumulated closely (Debye length $\sim$ 0.1 nm) around the nanotubes, and strong quenching might be expected.

Our device structure allows us to study the effect of the dielectric environment on charge transport in and emission from carbon nanotubes. As a quasi-one-dimensional object, the medium surrounding the nanotube has a strong influence on emission wavelength, peak width, and photoluminescence yield.[19,20] Increasing the dielectric constant ε leads to increased exciton screening and thus a decreased exciton binding energy. Simultaneously, the self-energy correction causes a red shift of emission that is larger than the blue shift associated with the reduced binding energy.[21,22] As charge screening increases with the dielectric constant of the surrounding medium, interband transitions (blue-shifted with respect to the exciton) become stronger and eventually dominate according to theory.[20] This has not yet been observed for photoluminescence from carbon nanotubes due to the strong luminescence quenching of nanotubes on solid substrates.[19,23,24] For electroluminescence, these limitations are less strict because very large numbers of excitons can be generated and thus light detection from individual nanotubes remains possible despite low efficiencies. For example, a small contribution of interband emission was recently assigned to unipolar impact excitation electroluminescence.[25,26] A very high ε dielectric that could lead to interband transitions is TiO_2 ($\varepsilon = 60-80$). However, TiO_2 is not very suitable as a thin gate dielectric on its own due to its relatively small band gap and thus high leakage. We will show that adding a thin layer (few nm) of TiO_2 or HfO_2 ($\varepsilon \approx 25$) to the electrolyte-gated carbon nanotube FETs allows us to significantly increase the dielectric constant of the nanotube environment without drastically altering the overall device and emission characteristics.

Figure 1a shows a schematic of the electrolyte-gated nanotube FET and the electroluminescence measurement setup. We fabricated aligned carbon nanotube transistors on quartz substrates with Ti/Pd source−drain electrodes (see inset Figure 1a) and a liquid electrolyte contacted with a PtIr wire as the gate electrode. Figure 1b,c shows current−voltage characteristics of nanotube array field-effect transistors gated *via* an electrolyte of either PEG:$LiClO_4$ or the ionic liquid 1-butyl-3-methylimidazolium octyl sulfate ($[BMIM]^+[octOSO_3]^-$). In both cases, ambipolar charge transport is evident for very low gate (V_g) and source−drain (V_{ds}) voltages with negligible hysteresis despite the very slow gate voltage sweep rate. Such extended bias stress typically leads to strong hysteresis in devices that use conventional oxide gate dielectrics. The limited gate modulation of the source−drain current (I_{ds}) is partially due to the ambipolar nature of the transport (*i.e.*, the hole and electron accumulation ranges overlap so that the channel is never in depletion) and to the presence of metallic nanotubes in the arrays. The point of minimum current roughly follows the expected $V_g = V_{ds}/2$ dependence for ambipolar FETs with threshold voltages near zero.[27] Effective peak mobilities for holes and electrons were calculated to range between 600 and 1200 $cm^2\ V^{-1}\ s^{-1}$ using $\mu = (\partial I_{ds}/\partial V_g) \cdot (L/(W \cdot V_{ds} \cdot C))$, with channel width W and channel length L. The devices capacitance C is determined using the quantum capacitance of a carbon nanotube with

one sub-band occupied ($C_q = 4 \times 10^{-10}$ F · m^{-1})[28] and the density of the nanotube array $\partial N/\partial W =$ 5−10 μm^{-1} minus the metallic tubes: $\partial N/\partial W =$ 3−7 μm^{-1} (N is the number of nanotubes in the channel) with $C_q \cdot \partial N/\partial W = 0.12 - 0.28$ μF · cm^{-2}. The effective capacitance of the electrolyte ($C_{el} >$ 10 μF · cm^{-2}) is orders of magnitude larger than the quantum capacitance of the array so that the total capacitance ($1/C = 1/C_{el} + 1/C_q$) is dominated by the latter.

The average maximum conductance per nanotube (including metallic SWNT) is on the order of 0.04 e^2/h (for $L = 10$ μm), which is comparable to values reported by Zhou *et al.* for nanotubes with diameters of 1.5 nm.[29] This value is within the average diameter distribution of the nanotube arrays determined by atomic force microscopy (AFM) and Raman spectroscopy (see Supporting Information Figures S1 and S2).

We note that, although imidazolium-based ionic liquids can disperse carbon nanotubes through weak van der Waals interactions,[30] we did not find evidence that the nanotubes become detached from the quartz surface when 1-butyl-3-methylimidazolium octyl sulfate is used as the electrolyte. Nevertheless, due to its comparatively large electrochemical operating window, we used PEG:LiClO$_4$ as the electrolyte for all experiments described in the following.

We observe light emission from electrolyte-gated carbon nanotube array transistors for a range of gate voltages, as a collection of emission spots, each of which corresponds to an individual nanotube in the array, as shown in Figure 2a. These emission spots appear to be nearly diffraction-limited with an isotropic full width at half-maximum of about 1.5 μm. For a source−drain voltage of −2.4 V, light emission appears at the source electrode for positive or small negative gate voltages (*e.g.*, for $V_g = 0$). Under these bias conditions, electrons accumulate over the entire length of the channel and hole injection at the source leads to recombination and emission along the edge of the electrode visible as a string of light spots. As the gate voltage shifts toward more negative values, the hole accumulation layer extends further away from the source. The point of charge recombination and emission for each nanotube shifts more into the channel and moves with decreasing gate voltage toward the drain (*e.g.*, $V_g = -1.2$ V in Figure 2a). The reverse movement takes place when the gate voltage increases again.

Figure 2b shows a composite image of emission from the device in Figure 2a. This image is created by assigning to each pixel the highest brightness value detected during the entire voltage sweep. In this way, traces of exciton recombination along the nanotubes become visible as well as apparently disconnected emission spots (see also Supporting Information Figure S3). The number of emission traces in Figure 2a is significantly smaller than one would expect from the nanotube density determined by SEM and AFM. One-third of the nanotubes are metallic and do not emit light. The observed movement of emission spots and increased brightness close to the contacts exclude the possibility of emission from metallic tubes due to Joule heating.[31] The diameter distribution of the aligned nanotubes (Supporting Information Figures S1 and S2) indicates that the majority emits at wavelengths longer than 1600 nm that are not detected by our InGaAs camera, which could account for the small number of observable emission spots compared to the density of aligned nanotubes estimated by SEM.

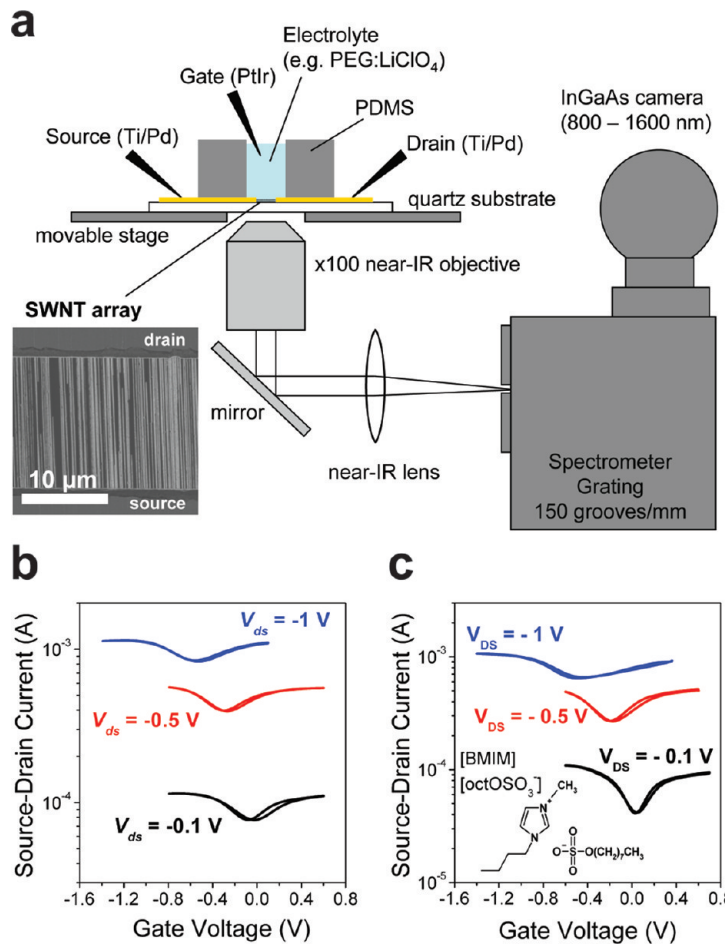

Figure 1. (a) Schematic illustration of device structure of an electrolyte-gated ambipolar carbon nanotube field-effect transistor and experimental setup for detection of near-infrared electroluminescence. FETs consist of an array of highly aligned single-walled carbon nanotubes on a double-side polished quartz wafer (thickness 500 μm) contacted with Ti/Pd source/drain electrodes (inset: scanning electron micrograph (SEM)). Emitted light is collected through the quartz substrate by a microscope objective and imaged onto a liquid nitrogen cooled InGaAs focal plane array. (b) Current−voltage characteristics of electrolyte-gated carbon nanotube FET with PEG:LiClO$_4$ electrolyte (channel length $L = 10$ μm, channel width $W = 150$ μm). (c) Current−voltage characteristics of electrolyte-gated carbon nanotube FET with ionic liquid, [BMIM]$^+$[octOSO$_3$]$^-$, electrolyte (channel length $L = 10$ μm, channel width $W = 150$ μm). In both cases, the gate voltage was scanned at 5 mV/s.

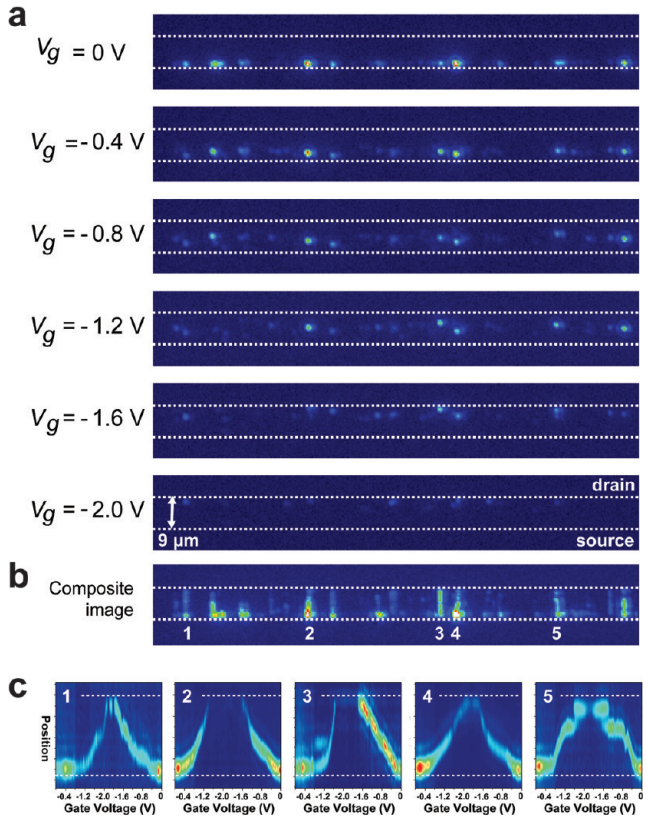

Figure 2. (a) False-color intensity images of electroluminescence from electrolyte (PEG:$LiClO_4$)-gated array of SWNT (L = 9 µm, W = 250 µm) for source−drain voltage V_{ds} = −2.4 V and different gate voltages (V_g). The white, dashed lines indicate the edges of the source and drain electrodes. (b) Composite image of light emission for entire gate voltage sweep illustrating the emission traces of individual nanotubes along the channel. (c) Position/intensity *versus* gate voltage maps for selected nanotubes in (b).

The average current density in these devices is on the order of 1−5 µA per nanotube. The distribution of current within the ensemble of nanotubes is determined by the conductance and contact resistance of metallic and semiconducting nanotubes with different diameters. The on-state conductance of semiconducting nanotubes is similar to that of metallic ones and increases linearly with nanotube diameter.[29,32] Higher injection barriers for larger band gap nanotubes and thus higher contact resistance further reduce the number of charges going through these nanotubes. Although this effect should be lower in electrolyte-gated devices compared to those with thick oxide dielectrics, it is likely to still play a role. We assume that these factors shift the distribution of current density toward large diameter nanotubes and thus decrease the probability of observing emission from smaller diameter nanotubes that emit within our detection range. Energy transfer to metallic or smaller band gap nanotubes[33] should not be a significant problem because nanotubes grown on quartz are almost perfectly aligned in parallel, and only very few of them form bundles or intersect with each other compared to random networks.

Devices with aligned arrays of SWNTs enable imaging of electroluminescence from many different nanotubes at a time and thus highlight the distribution of possible defects and emission efficiencies. Examples of position and intensity *versus* gate voltage plots are shown in Figure 2c. The movement of these light spots is reproducible for several voltage sweeps, and overall emission intensity increases with increasing source−drain voltage (see Supporting Information Figure S3). It is evident from Figure 2a,c that emission spots associated with individual nanotubes reach different positions along the channel for the same gate and source−drain voltage. We attribute these variations to the distribution of diameters and chiralities of nanotubes in the array resulting in different injection barriers and thus voltage drops at the contacts.[9]

In a simplified picture, we can assume diffusive transport and use the gradual channel approximation as shown by Tersoff *et al.*[16] to find the dependence of the emission spot position x_0 (as distance from drain) on V_g and V_{ds} including constant voltage drops at the source ($V_{C,s}$) and drain ($V_{C,d}$) electrodes to be

$$\frac{x_0}{L} = \frac{(V_{ds} - V_{C,d} - V_g)^2}{(V_{C,s} - V_g)^2 + (V_{ds} - V_{C,d} - V_g)^2} \qquad (1)$$

In the ambipolar regime, there is an overall voltage drop equal to the band gap due to the crossover from electron to hole conduction. Therefore $V_{C,s}$ and $V_{C,d}$ cannot be smaller than the Schottky barrier heights for holes and electrons, respectively. The emission zone moves from the source to the drain electrode within a gate voltage range of $V_{ds} - (V_{C,s} + V_{C,d})$.[16] This suggests that the larger voltage drops at the contacts with wide band gap (*i.e.*, small diameter) nanotubes should lead to a more rapid change of the emission zone position with gate voltage compared to small band gap (*i.e.*, large diameter) nanotubes. The difference between the voltage drop at the source and that at the drain electrode, the work function of Pd being closer to the SWNT valence band than the conduction band, should only cause an overall V_g shift of the curve compared to symmetric injection barriers (see Supporting Information Figure S4). Absolute values of hole and electron mobility do not have an impact on the movement of the emission zone provided that their ratio is close to unity, as is the case for our devices. According to this model, relative differences in motion of emission spots with gate voltage can be attributed to different voltage drops at the contacts and thus to different nanotube band gaps. This simple picture is complicated by the unknown gate voltage dependence of contact resistance and thus voltage drop at the contacts and the influence of electrolyte gating on it.

In order to study the light emission from carbon nanotubes embedded in high ε dielectrics, we deposited thin layers of HfO_2 (5 nm by atomic layer deposi-

tion, $\varepsilon \approx 25$, $C_{HfO_2} = 4.4\ \mu F \cdot cm^{-2}$) and TiO_2 (7 nm by electron beam evaporation, $\varepsilon \approx 60$, $C_{TiO_2} = 7.6\ \mu F \cdot cm^{-2}$) on top of the aligned carbon nanotubes as a buffer dielectric after the source/drain electrodes were patterned and before the device was completed as described earlier with the electrolyte and gate electrode. The capacitance of these thin buffer layers is still much higher than the quantum capacitance of the nanotubes, so that the overall efficiency of gating is not significantly decreased. Moreover, leakage through the electrolyte is greatly reduced, and device stability at higher voltages improved due to the separation of the source/drain electrodes from the electrolyte. The advantages of using electrolyte gating instead of a thin oxide as the only dielectric are simplified fabrication, high device yield, and reduction of leakage and dielectric breakdown especially for a high ε dielectric such as TiO_2 with a small band gap.

Figure 3a,b shows current−voltage characteristics of nanotube FETs with buffer layers of HfO_2 and TiO_2, respectively. They are overall similar to those of purely electrolyte-gated devices except for a threshold shift. In both cases, the transfer curves are shifted toward more positive gate voltages, which could indicate p-doping that occurred during the oxide deposition process or an increased contact resistance for electrons due to the additional dielectric. Despite this, we observe electroluminescence from these devices in a similar fashion as without the buffer layers. Examples are shown in Figure 3c (HfO_2) and Figure 4 (TiO_2). The same movement of emission spots from the source to the drain electrode takes place, and the intensity of emission from the individual nanotubes increases with source−drain voltage.

Again, using an array of nanotubes allows for observing emission from a range of nanotubes with different band gaps and possibly defects within a single device under uniform bias conditions. Panels 1 and 2 in Figure 3d show the position of light emission with changing gate voltage for two nanotubes. In panel 1, the emission zone moves from the source to the drain electrode over a gate voltage range of 1.3 V for a source−drain voltage of −2.8 V. This gives us a direct estimate of the voltage drop at the contacts because this voltage range equals $V_{ds} - (V_{C,s} + V_{C,d})$. The total voltage drop is 1.5 V, which is larger than any possible band gap of a nanotube in the array, based on the measured diameter distribution, but significantly smaller than values found for ambipolar FETs with small band gap nanotubes on SiO_2 dielectrics (5−6 V).[16] FETs without any buffer layer (see Figure 2c and Supporting Information Figure S3), and those with TiO_2 as the buffer dielectric (see Figure 4) exhibit similar contact-induced voltage drops. This is direct evidence that electrolyte gating significantly reduces contact resistance in carbon nanotube field-effect transistors. In Figure 3d, panel 2, the progression of emission zone position

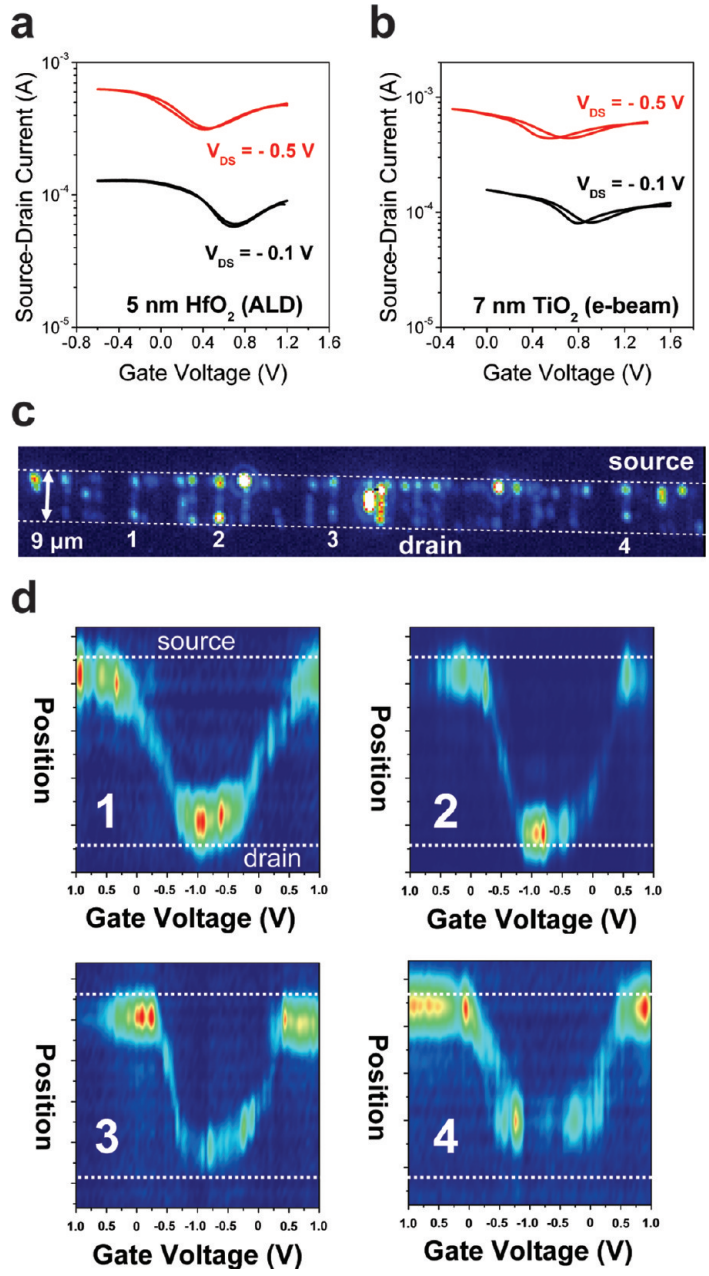

Figure 3. (a) Current voltage characteristics of electrolyte-gated SWNT-FET with additional 5 nm HfO_2 (ALD) buffer dielectric (L = 8 μm, W = 150 μm) and (b) 7 nm TiO_2 (e-beam) buffer dielectric (L = 8 μm, W = 150 μm). (c) Composite image of light emission for forward and reverse gate voltage sweep (V_g = 1.0 to −1.0 V, V_{ds} = −2.8 V) of electrolyte-gated FET of aligned carbon nanotubes (L = 9 μm, W = 250 μm) with a 5 nm buffer layer of HfO_2. (d) Position/intensity *versus* gate voltage maps for selected carbon nanotubes (1−4) in (c).

with gate voltage is much steeper than that in panel 1. A voltage difference of only 1 V covers the entire channel length. The overall voltage drop at the contacts therefore amounts to about 1.8 V, indicating that this nanotube has a larger band gap than the one in panel 1.

Besides emission from nanotubes with different band gaps, we observe emission traces that do not extend all the way across the channel but are confined to part of the channel, as shown in Figure 3d, panels 3

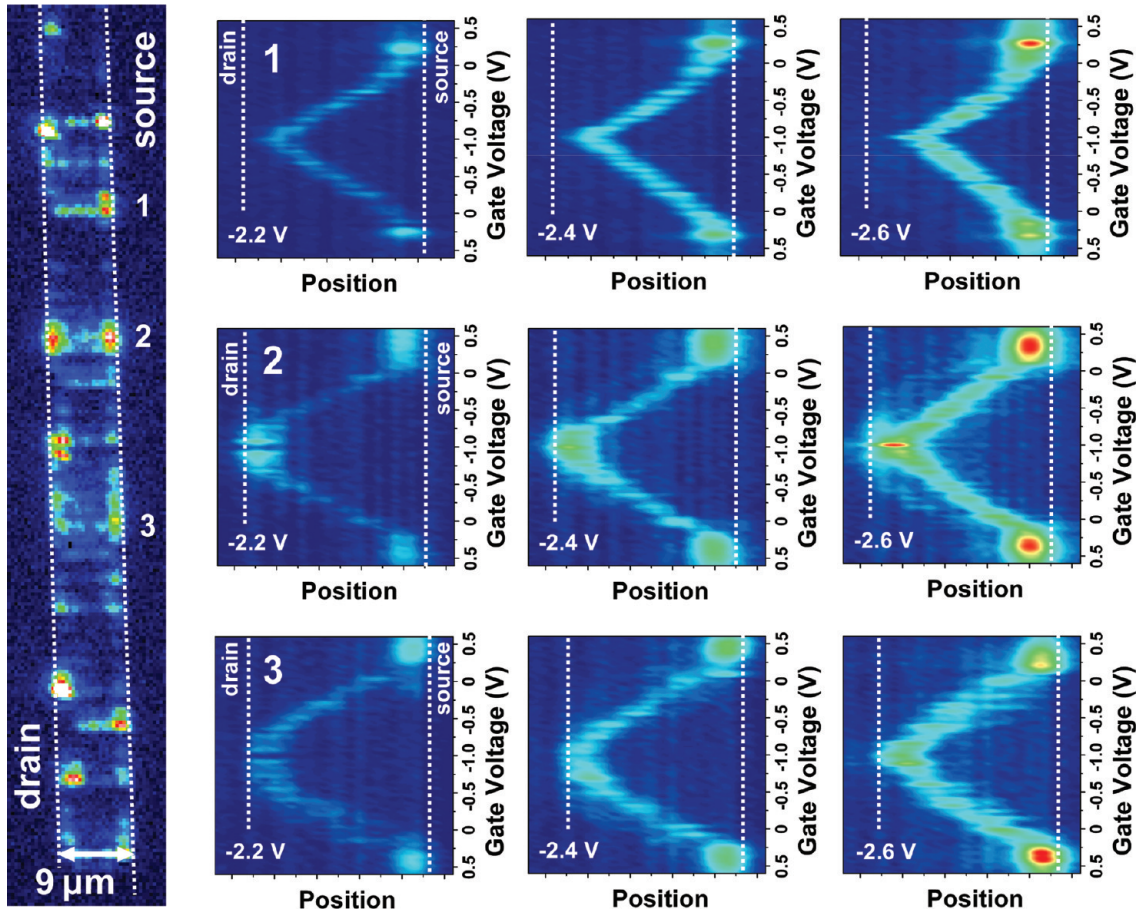

Figure 4. Left: composite image of light emission for forward and reverse gate voltage sweep (V_g = 0.6 to −1.0 V, V_{ds} = −2.4 V) of electrolyte-gated FET with aligned arrays of carbon nanotubes (L = 9 μm, W = 250 μm) and a buffer layer of 7 nm TiO_2. Right: position/intensity *versus* gate voltage plots of selected nanotubes (1−3) and their evolution with source−drain voltage (−2.2 to −2.6 V).

and 4. Various explanations are possible. A nanotube could change its chirality along the channel[19,34] and may emit outside the detection range from that point on. Alternatively, it could join a bundle, which would lead to energy transfer to smaller band gap nanotubes (Supporting Information Figure S1 shows a bundle of nanotubes that splits into well-separated nanotubes). Panel 4 in Figure 3d could be explained either way because emission disappears for more negative gate voltages before reoccurring at the same position when the voltage sweep is reversed. Another possible scenario for a shortened emission trace is the intersection of the emitting nanotube with a metallic nanotube and thus shorting out of the rest of the channel. The metallic nanotube then acts as an electrode itself. This could be the case in Figure 3d, panel 3, because here emission is continuous for the entire gate voltage sweep similar to a nanotube FET with shorter channel length.

Furthermore, we occasionally observe apparently disconnected emission spots within the channel region (see Figure 3c and Supporting Information Figure S3) that move little or not at all. Some of these emission spots emerge, move slightly, and disappear again with changing gate voltage. These could originate from short segments of nanotubes that are emissive within the detection range. Others that are stationary could result from defects (*e.g.*, sharp kinks as visible in AFM images, Supporting Information Figure S1) that can cause impact excitation and thus bright localized emission.[25,35]

In order to estimate the electroluminescence efficiency of electrolyte-gated SWNT-FETs, we need to correlate source−drain current with emission intensity. This can only be done for the entire device including the metallic and small band gap semiconducting nanotubes. As the gate voltage changes and thus alters the conductivity of the semiconducting SWNT, the distribution of current density among the ensemble of nanotubes is expected to change, as well. Figure 5 shows source−drain current and light output *versus* gate voltage characteristics for a purely electrolyte-gated FET and for one with a TiO_2 buffer layer. Due to the high source−drain bias (2−3 V) necessary to achieve detectable electroluminescence, the current modulation is small. For the FET without a buffer dielectric in Figure 5b, the emission intensity increases with decreasing gate voltage as more and more emission spots appear and move through the channel until they have reached

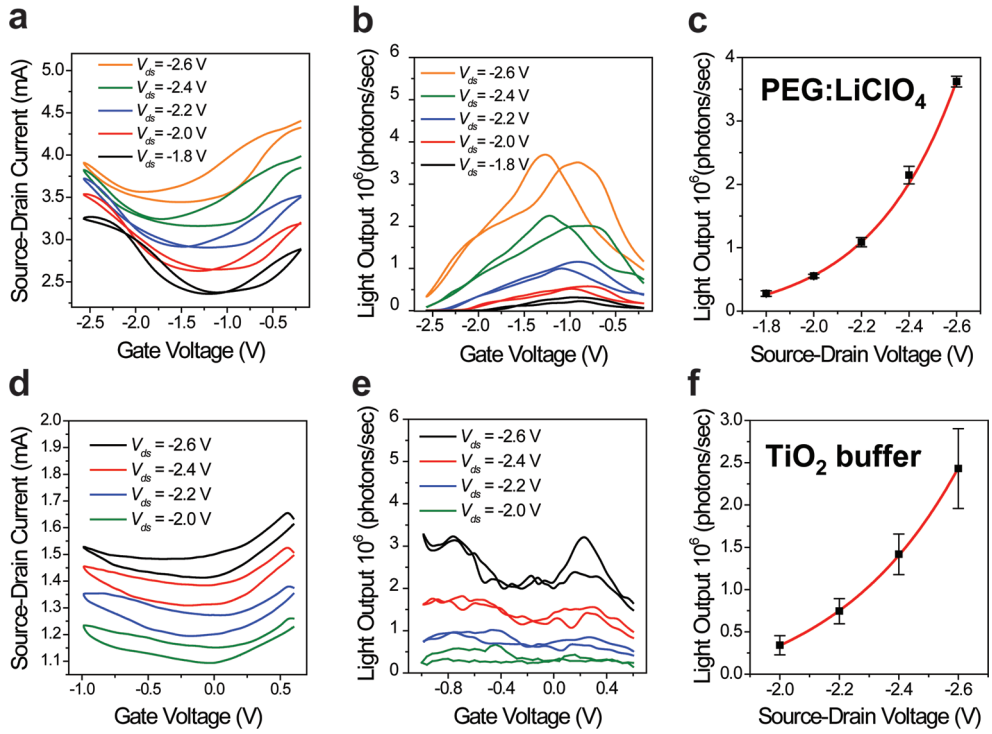

Figure 5. (a) Current−voltage characteristics of a SWNT-FET with PEG:LiClO$_4$ electrolyte (L = 6 μm, W = 150 μm). (b) Concurrent light output *versus* gate voltage for this device over the wavelength range of 800 to 1600 nm. (c) Average maximum light output (squares, error bars indicate maximum and minimum values) *versus* source−drain voltage and single exponential fit (red line). (d) Current−voltage and light output (e) *versus* gate voltage characteristics of an electrolyte-gated SWNT-FET (L = 9 μm, W = 250 μm) with TiO$_2$ buffer dielectric (7 nm). (f) Average maximum light output (squares, error bars indicate maximum and minimum values) *versus* source−drain voltage for this device and single exponential fit (red line).

the drain electrode and vanish as injection of electrons diminishes. For the device with a TiO_2 buffer layer, the total electroluminescence intensity remains relatively unchanged throughout the gate voltage sweep (Figure 5e), although emission from individual SWNT appears strongest close to the electrodes (see Figure 4). This may be explained by a broadening of the spectrum near the contacts and thus more photons within the detection range.[3] Alternatively, the increase of emission at the contacts could be a result of the lower mobility and thus higher concentration of carriers in the high-field region near the contact as suggested by McGuire *et al.*[36]

In both cases, the maximum emission intensity increases superlinearly with V_{ds} (Figure 5c,f), while I_{ds} increases more or less linearly. An exponential dependence of intensity on V_{ds}, which fits the data well, has previously been associated with impact excitation that is more efficient than ambipolar emission.[1,35,37] Although emission close to the electrodes (especially the source) is more intense than within the channel and increases more with V_{ds}, it is not stationary as one would expect for impact excitation[35] but vanishes when voltage conditions become more unipolar. Enhanced injection through the Schottky barrier at higher V_{ds} and thus larger carrier densities could also explain the observed V_{ds} dependence of the integrated emission intensity. This should also lead to higher source−drain currents, which may not show in the overall current−voltage characteristics due to the metallic nanotubes.

We estimate the effective external efficiency for devices with and without oxide buffers to be about 10^{-10} to 10^{-9} photons/electron. This is significantly lower than efficiencies found for ambipolar nanotube electroluminescence in previous studies.[4,5] We are, however, limited in detection to the wavelength range of 800 to 1600 nm. The diameter distribution of the CVD-grown SWNT is centered around 1.7 nm (corresponding to an emission wavelength of 2 μm), and only about 10−15% of all nanotubes is expected to emit within the detection range. Spectral resolution of a number of emission spots (Figure 6a−d) reveals that most of them represent only the high-energy tail of emission peaks beyond 1600 nm. This prevents a detailed analysis of the influence of the dielectric surrounding on the spectral distribution as well as correlation of emission behavior with nanotube diameter and band gap at this point. For very few emission spots, we could resolve a whole emission peak (Figure 6f). The width at half-maximum of these peaks varied between 50 and 100 nm (27−59 meV), which is significantly broader than photoluminescence peaks from CVD-grown suspended nanotubes (10−15 meV)[38] but similar to electroluminescence from other long channel devices (25 meV)[4] and narrower than those from short channel nanotube

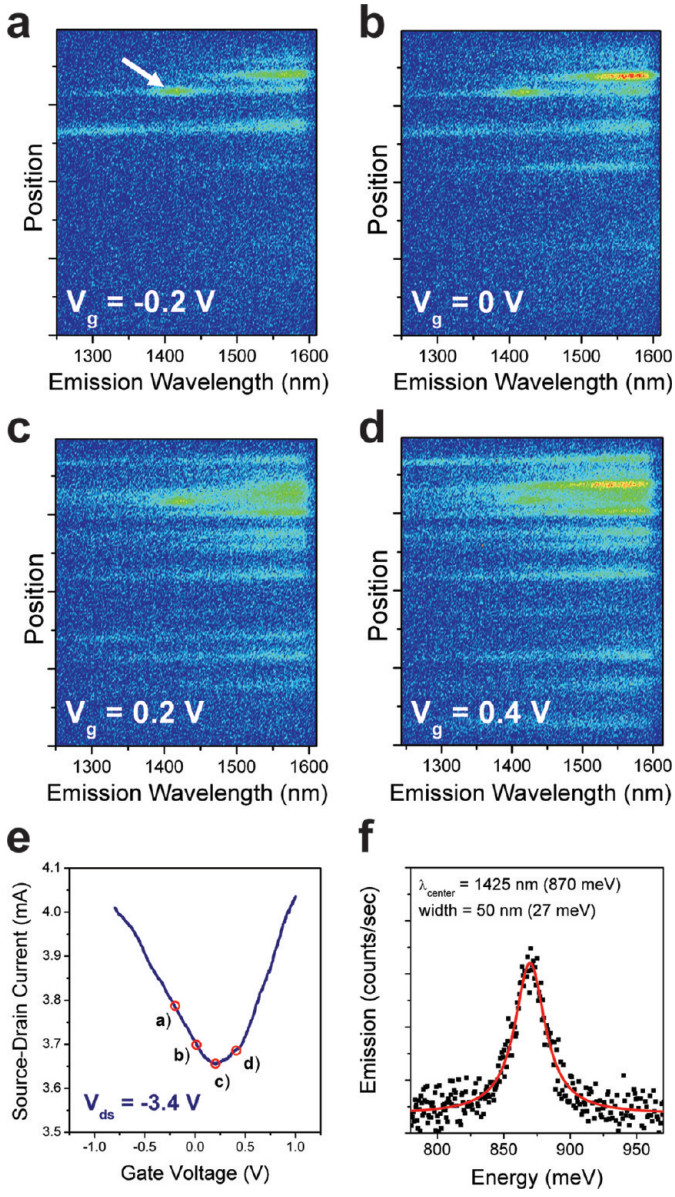

Figure 6. (a−d) Electroluminescence spectra of electrolyte-gated array of carbon nanotubes with 5 nm HfO_2 buffer layer ($V_{ds} = -3.4$ V, $L = 6$ μm, $W = 250$ μm). The spectrometer slit (perpendicular to nanotube orientation, parallel to electrode edge, slit width 200 μm) was positioned so that only emission from the middle of the channel was dispersed. The InGaAs camera sensitivity cutoff is at 1600 nm. (e) Current−voltage characteristics of device in (a)−(d). Circles indicate voltage conditions for each spectrum. (f) Resolved emission spectrum for emission spot indicated by white arrow in (a). Lorentzian peak fit (after subtraction of background) gives a peak center λ_{center} of 1425 nm (870 meV) and full width at half-maximum (fwhm) of 50 nm (27 meV).

FETs (80−100 meV).[5,39] Assuming this peak width range to be similar for all nanotubes regardless of diameter and taking into account the brightness of those emission spots for which only the high-energy tail of the spectrum was detected, we can estimate that the overall efficiency of these devices is much higher than 10^{-9} photons/electron. This is further supported by the fact that nanotubes with smaller band gaps exhibit more efficient carrier injection and higher mobilities and thus allow for higher current densities than nanotubes with larger band gaps and thus shorter emission wavelengths. Nevertheless, the differences of efficiency between FETs with and without dielectric buffer layers are within the margin of error of detection and device-to-device fluctuations. We thus conclude that emission from carbon nanotubes in direct contact with the electrolyte is not drastically more or less quenched than that from nanotubes embedded in an oxide.

In conclusion, we demonstrated near-infrared light emission from ambipolar electrolyte-gated field-effect transistors with dense parallel arrays of carbon nanotubes at exceptionally low gate and source−drain voltages and with minimal current hysteresis. The dependence of emission spot position and brightness on the applied voltages yielded information about the relative band gap, possible defects, and interactions of carbon nanotubes in the array and confirmed that electrolyte gating leads to low contact resistance for both charge carriers. Nanotube FETs using thin layers of HfO_2 or TiO_2 as high ε buffer dielectrics showed similar current−voltage and emission characteristics, opening a convenient way to study the influence of different dielectric media on carbon nanotube excitons. The estimated nanotube electroluminescence efficiencies did not significantly depend on the surrounding medium but were lower than previously reported values for ambipolar nanotube FETs on Si/SiO_2.[4,5] The demonstrated device structure is versatile and easy to fabricate with high yields. While the liquid electrolyte can be washed off for further analysis of the nanotubes, solid electrolytes could be employed for other applications. Increasing the ratio of semiconducting to metallic nanotubes and better control over the chirality and diameter distribution[40,41] will further improve device performance and electroluminescence yield of these near-infrared light-emitting FETs.

METHODS

We fabricated devices as shown in Figure 1a on double-side polished quartz wafers (ST-cut) whose annealed surface templates dense (1−10 SWNT/μm) and highly aligned growth of single-walled carbon nanotubes (see scanning electron micrograph, inset Figure 1a and Supporting Information Figure S1) from prepatterned submonolayer iron catalyst lines as described previously.[42] Evaporation and lift-off of Ti (1−2 nm)/Pd (30−40 nm) gave source and drain electrodes with channel lengths (L) of 5−15 μm and channel widths (W) of 150 and 250 μm. Oxide buffer layers were deposited by electron beam evaporation (TiO_2, thickness 7 nm) or by atomic layer deposition (HfO_2, at 120 °C with alternating pulses (50 cycles) of tetrakis(dimethylamido)hafnium(IV) precursor (0.06 s) and H_2O (0.6 s)). To complete the devices, a piece of polydimethylsiloxane (PDMS) elastomer with a trench was placed over the source and drain electrodes, so that the trench allowed access to the channel area while the larger parts of the electrodes were in conformal contact with the PDMS to reduce gate leakage. The trench was filled with the electrolyte, for example, polyethylene glycol methyl ether (PEG, Ald-

rich): $LiClO_4 \cdot 3H_2O$ (weight ratio 12:1) or the ionic liquid 1-butyl-3-methylimidazolium octyl sulfate (Aldrich). A PtIr wire immersed in the electrolyte acted as the gate electrode. Two Keithley 2400 source meters applied voltage to the gate and drain, while the source was grounded, and acquired current−voltage characteristics of the completed transistors. A near-infrared objective (Olympus LMPL 100xIR, NA = 0.8) collected light emitted through the quartz substrate (thickness 500 μm). The image was focused onto the entrance slit of a spectrometer (Acton SP150, focal length 15 cm) that enabled direct imaging with a mirror and spectral resolution with a grating (150 grooves/mm, blaze 1250 nm). A liquid nitrogen cooled InGaAs camera (Princeton Instruments 2D-OMA V) acquired images and spectra during voltage sweeps synchronized *via* a Labview interface. Each image was exposed and accumulated over a total of 60 s.

Acknowledgment. Device fabrication and electron microscopy were carried out at the Frederick Seitz Materials Research Laboratory Central Facilities, University of Illinois, which are partially supported by the U.S. Department of Energy under Grants DE-FG02-07-ER46453 and DE-FG02-07-ER46471. Nanotube characterization (Raman, AFM) and device measurements were performed at the Center for Nanoscale Materials, Argonne National Laboratory. The Center for Nanoscale Materials is supported by the U.S. Department of Energy, Office of Science, Office of Basic Energy Sciences, Contract DE-AC02-06CH11357.

Supporting Information Available: Atomic force microscopy and Raman analysis of the carbon nanotube diameter distribution and additional electroluminescence images. This material is available free of charge *via* the Internet at http://pubs.acs.org.

REFERENCES AND NOTES

1. Avouris, P.; Freitag, M.; Perebeinos, V. Carbon-Nanotube Photonics and Optoelectronics. *Nat. Photonics* **2008**, *2*, 341–350.
2. Misewich, J. A.; Martel, R.; Avouris, P.; Tsang, J. C.; Heinze, S.; Tersoff, J. Electrically Induced Optical Emission from a Carbon Nanotube FET. *Science* **2003**, *300*, 783–786.
3. Freitag, M.; Chen, J.; Tersoff, J.; Tsang, J. C.; Fu, Q.; Liu, J.; Avouris, P. Mobile Ambipolar Domain in Carbon-Nanotube Infrared Emitters. *Phys. Rev. Lett.* **2004**, *93*, 076803.
4. Freitag, M.; Perebeinos, V.; Chen, J.; Stein, A.; Tsang, J. C.; Misewich, J. A.; Martel, R.; Avouris, P. Hot Carrier Electroluminescence from a Single Carbon Nanotube. *Nano Lett.* **2004**, *4*, 1063–1066.
5. Adam, E.; Aguirre, C. M.; Marty, L.; St-Antoine, B. C.; Meunier, F.; Desjardins, P.; Menard, D.; Martel, R. Electroluminescence from Single-Wall Carbon Nanotube Network Transistors. *Nano Lett.* **2008**, *8*, 2351–2355.
6. Engel, M.; Small, J. P.; Steiner, M.; Freitag, M.; Green, A. A.; Hersam, M. C.; Avouris, P. Thin Film Nanotube Transistors Based on Self-Assembled, Aligned, Semiconducting Carbon Nanotube Arrays. *ACS Nano* **2008**, *2*, 2445–2452.
7. Kim, W.; Javey, A.; Vermesh, O.; Wang, O.; Li, Y. M.; Dai, H. J. Hysteresis Caused by Water Molecules in Carbon Nanotube Field-Effect Transistors. *Nano Lett.* **2003**, *3*, 193–198.
8. Aguirre, C. M.; Levesque, P. L.; Paillet, M.; Lapointe, F.; St-Antoine, B. C.; Desjardins, P.; Martel, R. The Role of the Oxygen/Water Redox Couple in Suppressing Electron Conduction in Field-Effect Transistors. *Adv. Mater.* **2009**, *21*, doi: 10.1002/adma.200900550.
9. Chen, Z. H.; Appenzeller, J.; Knoch, J.; Lin, Y. M.; Avouris, P. The Role of Metal−Nanotube Contact in the Performance of Carbon Nanotube Field-Effect Transistors. *Nano Lett.* **2005**, *5*, 1497–1502.
10. Kocabas, C.; Kim, H. S.; Banks, T.; Rogers, J. A.; Pesetski, A. A.; Baumgardner, J. E.; Krishnaswamy, S. V.; Zhang, H. Radio Frequency Analog Electronics Based on Carbon Nanotube Transistors. *Proc. Natl. Acad. Sci. U.S.A.* **2008**, *105*, 1405–1409.
11. Kang, S. J.; Kocabas, C.; Ozel, T.; Shim, M.; Pimparkar, N.; Alam, M. A.; Rotkin, S. V.; Rogers, J. A. High-Performance Electronics Using Dense, Perfectly Aligned Arrays of Single-Walled Carbon Nanotubes. *Nat. Nanotechnol.* **2007**, *2*, 230–236.
12. Siddons, G. P.; Merchin, D.; Back, J. H.; Jeong, J. K.; Shim, M. Highly Efficient Gating and Doping of Carbon Nanotubes with Polymer Electrolytes. *Nano Lett.* **2004**, *4*, 927–931.
13. Ozel, T.; Gaur, A.; Rogers, J. A.; Shim, M. Polymer Electrolyte Gating of Carbon Nanotube Network Transistors. *Nano Lett.* **2005**, *5*, 905–911.
14. Cho, J. H.; Lee, J.; He, Y.; Kim, B.; Lodge, T. P.; Frisbie, C. D. High-Capacitance Ion Gel Gate Dielectrics with Faster Polarization Response Times for Organic Thin Film Transistors. *Adv. Mater.* **2008**, *20*, 686–690.
15. Panzer, M. J.; Frisbie, C. D. High Carrier Density and Metallic Conductivity in Poly(3-hexylthiophene) Achieved by Electrostatic Charge Injection. *Adv. Funct. Mater.* **2006**, *16*, 1051–1056.
16. Tersoff, J.; Freitag, M.; Tsang, J. C.; Avouris, P., Device Modeling of Long-Channel Nanotube Electro-Optical Emitter. *Appl. Phys. Lett.* **2005**, *86*, 263108.
17. Guo, J.; Alam, M. A. Carrier Transport and Light-Spot Movement in Carbon-Nanotube Infrared Emitters. *Appl. Phys. Lett.* **2005**, *86*, 023105.
18. Brege, J. J.; Gallaway, C.; Barron, A. R. Fluorescence Quenching of Single-Walled Carbon Nanotubes in SDBS Surfactant Suspension by Metal Ions: Quenching Efficiency as a Function of Metal and Nanotube Identity. *J. Phys. Chem. C* **2007**, *111*, 17812–17820.
19. Lefebvre, J.; Austing, D. G.; Bond, J.; Finnie, P. Photoluminescence Imaging of Suspended Single-Walled Carbon Nanotubes. *Nano Lett.* **2006**, *6*, 1603–1608.
20. Perebeinos, V.; Tersoff, J.; Avouris, P., Scaling of Excitons in Carbon Nanotubes. *Phys. Rev. Lett.* **2004**, *92*, 257402.
21. Spataru, C. D.; Ismail-Beigi, S.; Capaz, R. B.; Louie, S. G. Quasiparticle and Excitonic Effects in the Optical Response of Nanotubes and Nanoribbons. *Carbon Nanotubes* **2008**, *111*, 195–227.
22. Finnie, P.; Homma, Y.; Lefebvre, J., Band-Gap Shift Transition in the Photoluminescence of Single-Walled Carbon Nanotubes. *Phys. Rev. Lett.* **2005**, *94*, 247401.
23. Iakoubovskii, K.; Minami, N.; Kazaoui, S.; Ueno, T.; Miyata, Y.; Yanagi, K.; Kataura, H.; Ohshima, S.; Saito, T. Ir-Extended Photoluminescence Mapping of Single-Wall and Double-Wall Carbon Nanotubes. *J. Phys. Chem. B* **2006**, *110*, 17420–17424.
24. Xie, L. M.; Liu, C.; Zhang, J.; Zhang, Y. Y.; Jiao, L. Y.; Jiang, L.; Dai, L.; Liu, Z. F. Photoluminescence Recovery from Single-Walled Carbon Nanotubes on Substrates. *J. Am. Chem. Soc.* **2007**, *129*, 12382–12383.
25. Chen, J.; Perebeinos, V.; Freitag, M.; Tsang, J.; Fu, Q.; Liu, J.; Avouris, P. Bright Infrared Emission from Electrically Induced Excitons in Carbon Nanotubes. *Science* **2005**, *310*, 1171–1174.
26. Avouris, P.; Freitag, M.; Perebeinos, V. Carbon-Nanotube Optoelectronics. *Carbon Nanotubes* **2008**, *111*, 423–454.
27. Radosavljevic, M.; Heinze, S.; Tersoff, J.; Avouris, P. Drain Voltage Scaling in Carbon Nanotube Transistors. *Appl. Phys. Lett.* **2003**, *83*, 2435–2437.
28. Rosenblatt, S.; Yaish, Y.; Park, J.; Gore, J.; Sazonova, V.; McEuen, P. L. High Performance Electrolyte Gated Carbon Nanotube Transistors. *Nano Lett.* **2002**, *2*, 869–872.
29. Zhou, X. J.; Park, J. Y.; Huang, S. M.; Liu, J.; McEuen, P. L., Band Structure, Phonon Scattering, and the Performance Limit of Single-Walled Carbon Nanotube Transistors. *Phys. Rev. Lett.* **2005**, *95*, 146805.
30. Wang, J.; Chu, H.; Li, Y. Why Single-Walled Carbon Nanotubes Can Be Dispersed in Imidazolium-Based Ionic Liquids. *ACS Nano* **2008**, *2*, 2540–2546.
31. Mann, D.; Kato, Y. K.; Kinkhabwala, A.; Pop, E.; Cao, J.; Wang, X. R.; Zhang, L.; Wang, Q.; Guo, J.; Dai, H. J. Electrically Driven Thermal Light Emission from Individual Single-Walled Carbon Nanotubes. *Nat. Nanotechnol.* **2007**, *2*, 33–38.
32. Tseng, Y. C.; Phoa, K.; Carlton, D.; Bokor, J. Effect of Diameter Variation in a Large Set of Carbon Nanotube Transistors. *Nano Lett.* **2006**, *6*, 1364–1368.

33. Qian, H. H.; Georgi, C.; Anderson, N.; Green, A. A.; Hersam, M. C.; Novotny, L.; Hartschuh, A. Exciton Energy Transfer in Pairs of Single-Walled Carbon Nanotubes. *Nano Lett.* **2008**, *8*, 1363–1367.
34. Anderson, N.; Hartschuh, A.; Novotny, L. Chirality Changes in Carbon Nanotubes Studied with Near-Field Raman Spectroscopy. *Nano Lett.* **2007**, *7*, 577–582.
35. Freitag, M.; Tsang, J. C.; Kirtley, J.; Carlsen, A.; Chen, J.; Troeman, A.; Hilgenkamp, H.; Avouris, P. Electrically Excited, Localized Infrared Emission from Single Carbon Nanotubes. *Nano Lett.* **2006**, *6*, 1425–1433.
36. McGuire, D. L.; Pulfrey, D. L. A Multi-Scale Model for Mobile and Localized Electroluminescence in Carbon Nanotube Field-Effect Transistors. *Nanotechnology* **2006**, *17*, 5805–5811.
37. Perebeinos, V.; Avouris, P., Impact Excitation by Hot Carriers in Carbon Nanotubes. *Phys. Rev. B* **2006**, *74*, 121410.
38. Lefebvre, J.; Fraser, J. M.; Finnie, P.; Homma, Y., Photoluminescence from an Individual Single-Walled Carbon Nanotube. *Phys. Rev. B* **2004**, *69*, 075403.
39. Xia, F. N.; Steiner, M.; Lin, Y. M.; Avouris, P. A Microcavity-Controlled, Current-Driven, on-Chip Nanotube Emitter at Infrared Wavelengths. *Nat. Nanotechnol.* **2008**, *3*, 609–613.
40. Ding, L.; Tselev, A.; Wang, J.; Yuan, D.; Chu, H.; McNicholas, T. P.; Li, Y.; Liu, J. Selective Growth of Well-Aligned Semiconducting Single-Walled Carbon Nanotubes. *Nano Lett.* **2009**, *9*, 800–805.
41. Ishigami, N.; Ago, H.; Imamoto, K.; Tsuji, M.; Iakoubovskii, K.; Minami, N. Crystal Plane Dependent Growth of Aligned Single-Walled Carbon Nanotubes on Sapphire. *J. Am. Chem. Soc.* **2008**, *130*, 9918–9924.
42. Kocabas, C.; Kang, S. J.; Ozel, T.; Shim, M.; Rogers, J. A. Improved Synthesis of Aligned Arrays of Single-Walled Carbon Nanotubes and Their Implementation in Thin Film Type Transistors. *J. Phys. Chem. C* **2007**, *111*, 17879–17886.